Available online at www.sciencedirect.com
ScienceDirect
Journal of Power Sources 172 (2007) 760–767
JOURNAL OF POWER SOURCES
www.elsevier.com/locate/jpowsour

Robust design of assembly parameters on membrane electrode assembly pressure distribution

Dong'an Liu [a], Xinmin Lai [a,*], Jun Ni [b], Linfa Peng [a], Shuhuai Lan [a], Zhongqin Lin [a]

[a] *School of Mechanical Engineering, Shanghai Jiaotong University, Shanghai 200240, People's Republic of China*
[b] *Department of Mechanical Engineering, University of Michigan, Ann Arbor, MI 48109-2125, USA*

Received 27 March 2007; received in revised form 10 May 2007; accepted 11 May 2007
Available online 24 May 2007

Abstract

The membrane electrode assembly (MEA) pressure distribution is an important factor that affects the performance of polymer membrane electrolyte fuel cell (PEMFC) stack. However, the general rules for assembly parameters that affect the MEA pressure distribution are hardly reported. In this study, a robust design analysis based on response surface methodology (RSM) was performed on a simplified fuel cell stack in order to identify the effect of assembly parameters on the MEA pressure distribution. The assembly pressure and bolt position were considered as randomly varying parameters with given probabilistic property and acted as the design variables. The max normal stress and normal stress uniformity of the MEA were determined in terms of the probabilistic design variables. The reliability of the robust design has been verified by comparing the robust solution with the optimal solution and an arbitrary solution.

Keywords: Robust design; RSM; Error propagation equation; Desirability function

1. Introduction

Fuel cells are recognized as potentially environmentally friendly power sources for residential, portable and transportation applications [1]. The interest in the usage of PEMFC in a variety of power generation applications is increasing every day, which makes the performance improvement, economical and energy efficiency of fuel cell necessary. In a single PEMFC, a MEA is sandwiched between two bipolar plates housing the flow channels. Multiple fuel cells are stacked together in most practical applications to provide sufficiently high power and desired voltage. This configuration results in the amplification of the losses from contact resistance between contacting components [2].

According to the former researches, one of the most important factors that affect the contact resistance is the component pressure distribution of PEMFC stack. For PEMFC stacks using common graphite bipolar plates which are not flexible, increasing the pressure on MEA leads to increasing the electric conductivity and reducing the permeability of the assembly [3]. However, the brittle gas diffusion layer can be damaged if too much pressure is applied. There have been some PEMFC stacks reported using flexible bipolar plates. For example, Yan et al. [4] developed a type of cheap expanded graphite plate material and a production process for fuel cell bipolar plates. They successfully assembled 1 and 10 kW stacks using the expanded graphite bipolar plates. Hwang and Hwang [5] assembled a double-cell PEMFC using Grafoil^{TM} flow-field plates and studied the performance of the stack. For these flexible bipolar plate designs, not only the MEA pressure distribution but also the bipolar plates pressure distribution are very important. To some extent, the latter is more important. In this study, we mainly focus on the PEMFC stacks using common graphite plates. As to these stacks, because of the relatively thin dimensions and low mechanical strength of the MEA versus bipolar plates and end plates, and the requirement of small contact resistance, the most important goal in the stacking design and assembly is to achieve a proper and uniform MEA pressure distribution [6].

Lee et al. [6] proposed a finite element analysis (FEA) model and analyzed the MEA pressure distribution under given assembly pressure. They demonstrated that the point-load stacking design was not a good method for obtaining a uniform pressure

* Corresponding author. Tel.: +86 2134206303; fax: +86 2134206340.
E-mail address: xmlai@sjtu.edu.cn (X. Lai).

0378-7753/$ – see front matter © 2007 Elsevier B.V. All rights reserved.
doi:10.1016/j.jpowsour.2007.05.066

distribution. Lee et al. [7] reported the changes in fuel cell performance as a function of the compression pressure resulting from torque on the bolts that clamped the fuel cell. Yoon et al. [8] and Mishra et al. [2] conducted some experiments on measuring the contact resistance under different assembly pressure. Vlahinos et al. [3] first gave a model considering the material and manufacturing variations. They analyzed the effects of these variations on MEA pressure distribution. Zhou et al. [9] studied the influence of the clamping force on the performance of PEMFC and made the conclusion that there would be a maximum power density if an optimal clamping force is found for a practical fuel cell system. For other fuel cell types, such as the solid oxide fuel cell stacks, the pressure distribution also has effect on the contact resistance. Koch and Hendriksen [10] investigated the load behavior of the contact resistance and found a power law dependence between the load and the contact resistance on a solid oxide fuel cell stack. The conclusion was drawn that contact resistance over an interface is highly dependent on the contact load.

Nevertheless, the general rules for assembly parameters that affect the MEA pressure distribution have been seen in almost none report. For example, the amount of assembly pressure has been always determined by the trial-and-error process. On the other hand, the end plate assembly bolts may be located at the four corners or at the middle of four margins of the end plate. Furthermore, in reality, there are always variations in the assembly parameters. It is neither physically possible nor financially feasible to completely eliminate the variations. Therefore, the need exists to identify the robust solution for assembly parameters that can produce the best MEA pressure distribution and are also insensitive to the variations in the assembly parameters.

In this study, it is aimed to investigate the effects of the assembly pressure and the position of end plate bolts on the MEA pressure distribution. A numerical model of a PEMFC stack was developed and the robust solution of the assembly parameters was achieved through the methodology described in this paper.

2. Methodology

The main purpose of this research is to develop a methodology and a FEA simulation procedure to establish the numerical tools for the evaluation of the stack design and cell assembly parameters. The schematic plot of the methodology is shown in Fig. 1, which is composed of a numerical modeling procedure and a robust design process.

The well-established finite element method was employed for the numerical model. At first, the dimensions of all fuel cell components were collected to construct the CAD model. Then, the mechanical properties, the loading and boundary conditions, and the behavior of the contacting interface of the components must be consistent with the actual physical situation. Finally, the proper types of elements for each component and their interfaces must be selected to allow a realistic physical behavior. Meshing is also important to obtain an accurate result. The significant difference in thickness between the components requires a special consideration in the meshing scheme. During the creation of the finite element method (FEM) model, all the dimensions, loading and boundary conditions, and mechanical properties are fully parameterized. Since the type and amount of assembly pressure depends on the type of stacking designs, the FEM model developed above is designed to be able to simulate different stacking designs and compression methods. For example, by applying the assembly pressure on the top surface of the end plate, the model can be used to simulate the "surface-load" stacking design. By adding the number of assembly bolts, the model can also be used to simulate the "line-load" stacking design.

In order to find the robust solution of the assembly parameters, a robust design process was developed. The RSM was used to establish the response variables in a form of second-order polynomial of the design variables. After establishment of the second-order polynomial, the transmitted variation in the design variables can be obtained using the error propagation equation (POE). At last, an overall desirability function was formed by

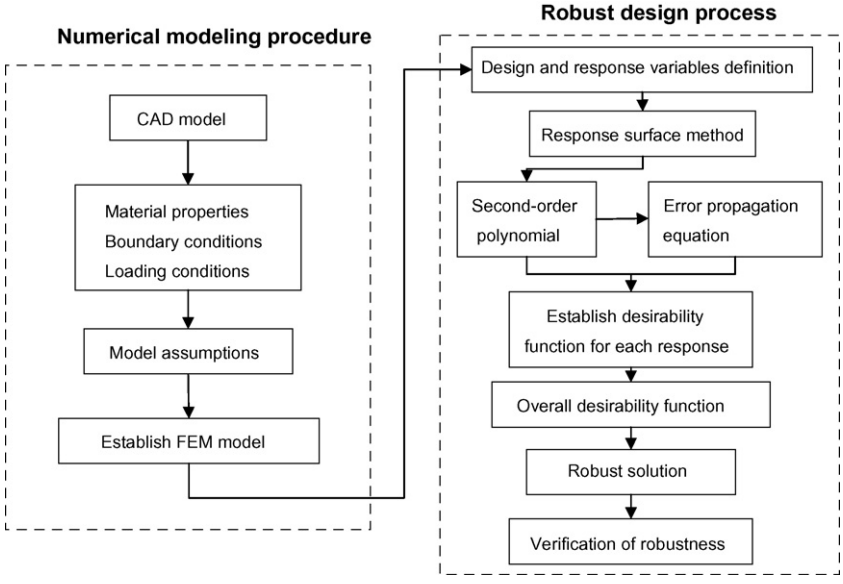

Fig. 1. Schematic plot of the simulation methodology.

combining the single desirability function of each response. By maximizing the overall desirability function, the robust solution was obtained. After verification of robustness, the established numerical simulation procedures can be used to evaluate a new stacking design and/or optimize cell assembly parameters.

3. Numerical model for a PEMFC stack

A typical PEMFC stack consists of a pair of end plates, several bipolar plates and several MEAs. Each MEA is sandwiched between two bipolar plates. On the end plate, four bolts hold the stack together by imposing certain pressure.

In this study, a two-cell stack model was developed and the FEM model is shown in Fig. 2. The commercial code of ANSYS was used to build the FEM model. The 3D elements solid 45 and solid 95 were used to represent the bipolar plate, the MEA and the end plate, where solid 45 and solid 95 are popular element types that can be used for 3D modeling of solid structures. Solid 45 is defined by eight nodes having three degrees of freedom at each node and solid 95 defined by 20 nodes having three degrees of freedom per node is a higher-order version of solid 45. A combination of mapped meshing and automatic meshing was adopted in order to ensure proper element connectivity and a correct aspect radio. The interfacial nodes between the bipolar plate and the MEA, and between the end plate and the bipolar plate were coupled in the normal direction to model the contact behavior as shown in Fig. 2(A).

The assembly pressure was applied through four bolt and nut assemblies. To simplify the numerical model, the bolts and nuts were ignored in the finite element model. The assembly pressure was applied directly at the contacting areas of the end plate as shown in Fig. 2(B). The FEM model has to be properly constrained in order to prevent the free movement. Due to the symmetry of the stack, half of the stack was employed in the analysis and the symmetrical boundary conditions were applied at the bottom side of the model.

The bolt position and the assembly pressure are both parameterized. The elements are color-coded based on their material properties. The dimension and mechanical property of each component is listed in Table 1. The mechanical properties of the components are cited from Ref. [3]. In practice, bipolar plates and MEA can be anisotropic due to either their structures or manufacturing processes. However, our simulation is a 3D structure analysis and the anisotropic material behavior is complicated and time consuming for the simulation. Thus, to simplify the model, the material behavior was assumed isotropic. The model involved the following assumptions:

(1) The small fillets were ignored.
(2) The effect of gravity was neglected.
(3) The material behavior was assumed to be linear elastic and isotropic.

Table 1
Dimension and mechanical property of each component [3]

Component	Modules of elasticity (MPa)	Poisson's ratio	Size (mm)
End plate	70,000	0.3	$84 \times 84 \times 8$
MEA	21	0.001	$50 \times 50 \times 0.457$
Bipolar plate	5,100	0.3	$50 \times 50 \times 1.27$

4. Robust design process for assembly parameters

4.1. Design and response variables definition

As shown in Fig. 3, the bolt position can be expressed as the vertical position dimension Pos_x and the horizontal position dimension Pos_y. Since Pos_x is usually much smaller than Pos_y, we mainly focus on the effect of different Pos_y on the MEA pressure distribution, with Pos_x being kept as constant. The translation directions of the four bolts position are shown by the arrows in Fig. 3. Because the end plate is foursquare and the translation of the four bolts are at the same time, the Pos_y of one bolt can represent the other three bolts'.

In this study, the bolt position Pos_y and the assembly pressure P were considered as randomly varying parameters with given distribution type and acted as the design variables. The normal stress and the normal stress uniformity were determined in terms

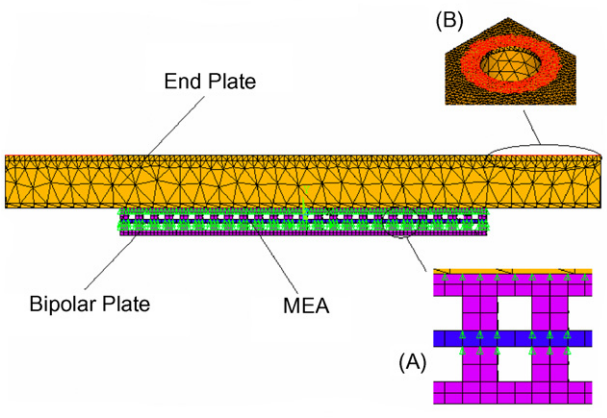

Fig. 2. (A and B) Half of the finite element model of a two-cell PEMFC stack.

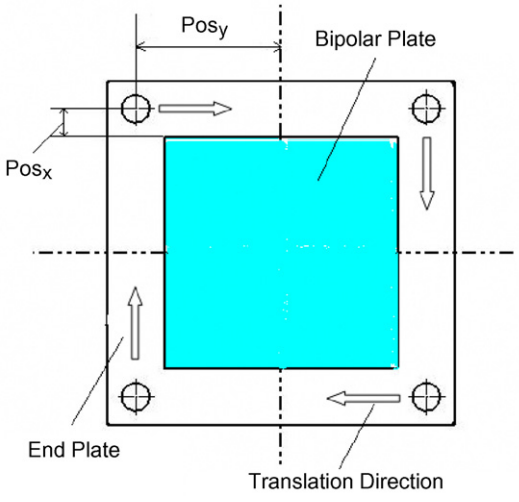

Fig. 3. Schematic of the translation of bolt position.

Table 2
Probabilistic properties of the design variables and the coded design variables

Variables[a]	Lower	Upper
Pos_y (mm)	0	33.5
P (MPa)	0	1.5
Coded Pos_y (mm)	−1.4285	1.4285
Coded P (MPa)	−1.4285	1.4285

[a] All variables are assigned uniform distribution between the lower and upper limits, respectively.

of the probabilistic design variables. The membrane's maximum and minimum compression stress $\max\sigma_z$ and $\min\sigma_z$ can be easily found. The difference between maximum and minimum compression stress can be defined as the differential compression stress in the membrane $\Delta\sigma_z$. $\max\sigma_z$ represents the value of contact pressure and $\Delta\sigma_z$ represents the uniformity of MEA pressure distribution. When $\max\sigma_z$ increases, it means the contact pressure on MEA becomes larger. If $\Delta\sigma_z$ increases, the uniformity of MEA pressure distribution will become worse.

According to the dimension of the end plate and the engineering need, two design spaces for the two design variables were established, respectively. The random distribution types for the design variables must be chosen carefully in the design space so as to reveal the actual distributions of the design variables. Within a certain interval in the design space, we consider each value of the design variable makes the same contribution to the establishment of the response surface. That means any level of the design variables can be the robust solution equally. Since the "uniform distribution" is a very fundamental distribution for cases where there is no evidence that any value of the random variable is more likely than any other in the design space, we assign the uniform distribution for the design variables in the design space. Probabilistic properties of all the design variables are listed in Table 2. The response variables are $\max\sigma_z$ and $\Delta\sigma_z$.

4.2. Response surface establishment

In order to find the relationship between the design variables and the response variables, the RSM was utilized. RSM is a combination of statistical and mathematical techniques, which is useful for developing, improving, and optimizing process [11]. A second-order model is commonly used for the multidisciplinary design in RSM. In general, the response model can be written as follows:

$$y(x) = \beta_0 + \mathbf{x}^{\mathrm{T}}\mathbf{b} + \mathbf{x}^{\mathrm{T}}\mathbf{B}\mathbf{x} \tag{1}$$

where β_0, $\mathbf{b}$, $\mathbf{B}$ are coefficients or coefficient matrices for design variables $\mathbf{x}$.

The central composite design (CCD) is a popular method that can be effectively applied to construct the second-order model for RSM [12]. To fulfill the CCD, probabilistic design system (PDS) was used. PDS is an analysis technique for assessing the effect of uncertain input parameters and assumptions on the model. It can account for the randomness in input variables such as material properties, boundary conditions, loads and geometry [13]. In PDS, statistical distribution functions (such as the Gaussian, the uniform distribution, etc.) describe uncertain parameters. For a given set of the distribution parameters of the design variables and the assumed distributions, one can generate a large set of random numbers for each variable using PDS [14]. In PDS, the CCD is fully automated and execution of CCD on the numerical model developed in Section 3 will result in a set of the response attributes. The results of CCD are listed in Table 3.

Two second-order polynomial models in the form of Eq. (1) were fitted to the data. The items/effects that are not significant (confidence level = 95%) were stepped down from the models using forward-stepwise-regression without damaging the model hierarchy. The values of regression coefficients were calculated and the fitted equations (in terms of coded values) for $\max\sigma_z$ and $\Delta\sigma_z$ are

$$\max\sigma_z = 0.341 + 0.056x_1 + 0.236x_2 + 0.043x_1x_2 \tag{2}$$

$$\Delta\sigma_z = 0.218 + 0.076x_1 + 0.158x_2 + 0.016x_1^2 + 0.057x_1x_2 \tag{3}$$

where x_1 and x_2 are the coded values of Pos_y and P. The probabilistic properties of x_1 and x_2 are listed in Table 2. The coding equations are

$$x_1 = 0.085\,Pos_y - 1.429; \qquad x_2 = 1.905\,P - 1.429 \tag{4}$$

Analysis of variance (ANOVA) was conducted to determine the significance of the fitted regression models. Significance was judged by determining the probability level that the F-statistic calculated from the data is less than 5%. The F-statistic equation is

$$F = \frac{\mathrm{SSR}/(m-1)}{\mathrm{SSE}/(n-m)} \tag{5}$$

where SSR is the sum of squares due to regression and SSE is the sum of squares of the residuals. n is the number of experiments and m is the number of terms in the fitted model. SSR and SSE are computed as

$$\mathrm{SSR} = \sum_{i=1}^{n}(\hat{y}_i - \bar{y})^2; \qquad \mathrm{SSE} = \sum_{i=1}^{n}(y_i - \hat{y}_i)^2 \tag{6}$$

where $\hat{y}_i$ represents the ith response value predicted by the fitted model and $\bar{y}$ represents the average response value.

Table 3
Results of CCD

Loop	Pos_y (mm)	P (MPa)	$\max\sigma_z$ (MPa)	$\Delta\sigma_z$ (MPa)
1	16.75	0.7500	0.3305	0.2176
2	0.1675	0.7500	0.2811	0.1497
3	33.33	0.7500	0.4240	0.3481
4	16.75	0.0075	0.0033	0.0022
5	16.75	1.4925	0.6577	0.4330
6	5.024	0.2250	0.0846	0.0460
7	28.48	0.2250	0.1213	0.0947
8	5.024	1.275	0.4797	0.2605
9	28.48	1.275	0.6875	0.5364

The total variation of the response data, SST (total sum of squares) is computed as

$$\mathrm{SST} = \mathrm{SSR} + \mathrm{SSE} = \sum_{i=1}^{n} (y_i - \bar{y})^2 \tag{7}$$

R^2 is an accompanying statistic to the F-statistic. It expresses the proportion of the variation of y_i from the model and the experimental data about the mean $\bar{y}$. Another useful measure is the adjusted R^2 statistic R_A^2:

$$R^2 = \frac{\mathrm{SSR}}{\mathrm{SST}}; \qquad R_A^2 = 1 - \frac{\mathrm{SSE}/(n-m)}{\mathrm{SST}/(n-1)} \tag{8}$$

The ANOVA for the refined models is summarized in Table 4. Because of $F(3, 5, 0.05) = 5.41$, $F(4, 4, 0.05) = 6.39$, the F-value of $796 > F(3, 5, 0.05)$ for $\max\sigma_z$ and $831 > F(4, 4, 0.05)$ for $\Delta\sigma_z$ imply the two models are significant at 95% confidence level. On the other hand, R^2 and R_A^2 were calculated to check the model adequacy. A high proportion of variability ($R^2 > 0.9$) in the response models can be explained successfully by the models (Eqs. (2) and (3)). However, a large value of R^2 does not always imply that the regression model is a good one. Adding a variable to the model will always increase R^2, regardless of whether the additional variable is statistically significant or not. Thus, there is a need to use a R_A^2 to evaluate the model adequacy and should be over 90%. Table 4 shows that R^2 and R_A^2 values for the models do not differ dramatically. This can be an indication that insignificant terms have not been included in the models.

To visualize the combined effect of the two design variables on the responses, the response surfaces and contour plots were generated for each of the fitted models. Fig. 4 shows the effect of Pos_y and P on $\max\sigma_z$ and $\Delta\sigma_z$.

As clear from Fig. 4(a), the maximum response for $\max\sigma_z$ occurs when Pos_y and P are at their highest level. Increasing P rises up $\max\sigma_z$ rapidly, which is in accordance with Lee's results [6]. This suggests that the assembly pressure P has a very significant effect on the MEA pressure distribution. It can be seen that the response also verifies noticeably at different levels of Pos_y, especially when the assembly pressure P is larger. With P fixed and Pos_y increased, $\max\sigma_z$ also becomes larger, which means the assembly bolts at the corner of end plate produce larger $\max\sigma_z$ than other positions with the same assembly pressure.

In this study, since $\Delta\sigma_z$ represents the uniformity of the MEA pressure distribution and smaller value of $\Delta\sigma_z$ means better uniformity, the $\Delta\sigma_z$ is subjected to be minimized. As shown in Fig. 4(b), the increase of $\Delta\sigma_z$ is slower at the lower level of P and Pos_y than the higher level, and smaller value can be gained at

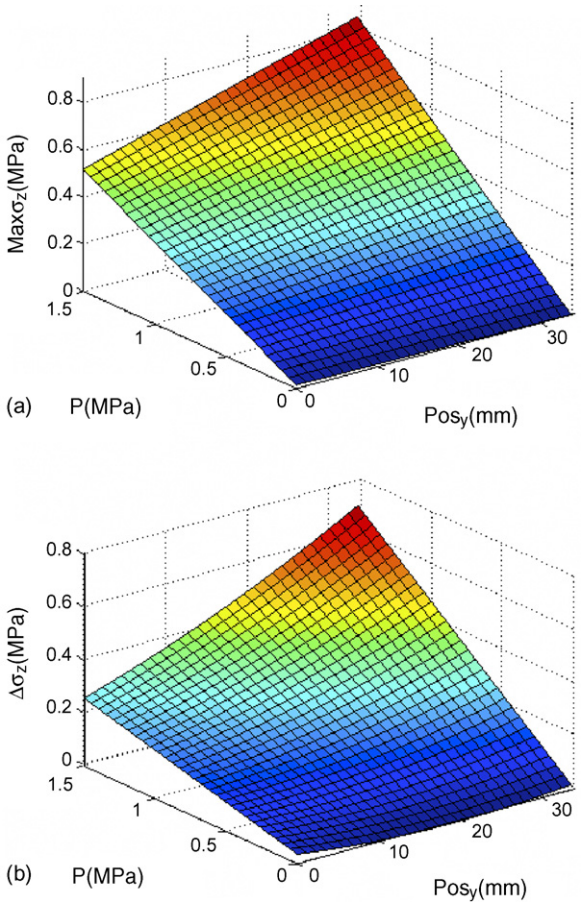

Fig. 4. Response surfaces and contour plots for (a) $\max\sigma_z$ and (b) $\Delta\sigma_z$.

the lower level of P and Pos_y. It can also be seen from Fig. 4 that the two response variables $\max\sigma_z$ and $\Delta\sigma_z$ are competing with each other, which means we cannot get a larger $\max\sigma_z$ while keeping $\Delta\sigma_z$ smaller simultaneously as we expect.

4.3. Error propagation equations establishment for response variables

The design may not achieve the desired result due to the influence of uncontrollable noise and variation of the input factors [15]. Therefore, designs are sought that are not only optimal but also robust (insensitive) to inevitable changes in the noise and input factors. To accomplish this objective, one should set the controllable factors to the levels that reduce variation in the response: (1) caused by the variation in the uncontrollable factors [16] and (2) transmitted from variation in the controllable

Table 4
ANOVA for the refined models

Source	$\max\sigma_z$					$\Delta\sigma_z$				
	d.f.	Sum of squares	F	R^2	R_A^2	d.f.	Sum of squares	F	R^2	R_A^2
Regression	3	0.4772				4	0.2601			
Residual	5	9.99×10^{-4}	796	0.9979	0.9967	4	5.22×10^{-4}	831	0.9980	0.9968
Total	8	0.4782				8	0.2606			

factors [17]. In this research, we mainly focused on reducing transmitted variation in the controllable factors.

Desirability-based robust design is a tool to find the controllable factor settings that optimize the objective yet minimize the response variation of the design [15]. It requires construction of a response surface using a mathematical model (Eq. (1)). The variation transmitted to the response can be determined by the well-known error propagation equation, which is modeled by taking the partial derivatives of the polynomial (Eq. (1)) with respect to the design variables:

$$\mathrm{POE} = \sigma_y = \left[\sum_{i=1}^{n}\left(\frac{\partial y}{\partial x_i}\right)^2 \sigma_{x_i}^2 + \sigma_{\mathrm{resid}}^2\right]^{1/2} \tag{9}$$

where σ_y is the model-predicted standard deviation of the response y, $\sigma_{x_i}^2$ the variance of design variable x_i and σ_{resid} is the residual variance.

The two POE for max σ_z and $\Delta\sigma_z$ were calculated based on Eqs. (2), (3) and (9) with the standard deviation in P set as $\sigma_P = 0.04$ MPa, in Pos_y set as $\sigma_{\mathrm{Pos}_y} = 0.33$ mm and the residual variance set as 0:

$$\mathrm{POE}_1 = (3.253 + 1.171x_1 + 0.038x_2 + 0.106x_1^2 + 0.015x_2^2)^{1/2} \times 10^{-2} \tag{10}$$

$$\mathrm{POE}_2 = (1.498 + 1.081x_1 + 0.068x_2 + 0.195x_1^2 + 0.026x_2^2 + 0.028x_1x_2)^{1/2} \times 10^{-2} \tag{11}$$

where x_1 and x_2 are the coded values of Pos_y and P. POE_1 and POE_2 are the standard deviation of maxσ_z and $\Delta\sigma_z$, respectively.

To reduce the variance in the response, POE should be minimized, therefore, it can be treated as an additional response built into the design process. The simultaneous optimization of several responses (in this case, maxσ_z, $\Delta\sigma_z$, POE_1 and POE_2) is the essence of the desirability-based robust design [17,18].

4.4. Desirability function

Desirability function is based on the idea that the "quality" of a product or process that has multiple quality characteristics, with one of them outside of some "desired" limits, is completely unacceptable. The method finds operating conditions x that provide the "most desirable" response values. Depending on whether a particular response y_i is to be maximized or minimized, different desirability functions $d_i(y_i)$ can be used. Let L_i, T_i and U_i be the lower, target and upper values, respectively, that are desired for response y_i with L_i, T_i and U_i [19].

If a response is to be maximized, its individual desirability function is with the exponent S determining how important it is to hit the target value. For $S = 1$, the desirability function increases linearly towards T_i which denotes a large enough value for the response; for $S < 1$, the function is convex, and for $S > 1$, the function is concave [19]:

$$d_i(y_i) = \begin{cases} 0, & y_i(x) < L_i \\ \left(\dfrac{y_i(x) - L_i}{T_i - L_i}\right)^s, & L_i \le y_i(x) \le T_i \\ 1, & y_i(x) > T_i \end{cases} \tag{12}$$

If a response is to be minimized, its individual desirability function is with T_i denoting a small enough value for the response:

$$d_i(y_i) = \begin{cases} 1, & y_i(x) < T_i \\ \left(\dfrac{y_i(x) - U_i}{T_i - U_i}\right)^s, & T_i \le y_i(x) \le U_i \\ 0, & y_i(x) > U_i \end{cases} \tag{13}$$

where T_i represents a small enough value for the response.

A single overall desirability index D can be obtained by combining the desirability value of each response. By assigning a range of numbers, for example 1–5, to the importance of optimizing each response variable, the weighing coefficients can be further refined. The final desirability index then is computed as follows:

$$D = (d_1^{w_1} \times d_2^{w_2} \times d_3^{w_3} \times \cdots \times d_n^{w_n})^{1/\sum w_i} = \left(\prod_{i=1}^{n} d_i^{w_i}\right)^{1/\sum w_i} \tag{14}$$

where w_i is a number indicating the relative importance of the ith response, which might typically be an integer in the range of 1–5, with 5 indicating the most importance and 1 indicating the least importance [19].

In this study, the two responses maxσ_z and $\Delta\sigma_z$ were scaled to the desirability functions d_1 and d_2 ranged from [0,1] by Eqs. (2), (3), (12) and (13) with $T_1 = 0.4$, $L_1 = 0.8$, $T_2 = 0.1$ and $U_2 = 0.5$, where maxσ_z and $\Delta\sigma_z$ are subjected to be maximized and minimized, respectively. POE_1 and POE_2 were also scaled to two desirability functions d_3 and d_4 according to Eqs. (10), (11) and (13) with $T_3 = 0.01$, $U_3 = 0.02$, $T_4 = 0.005$ and $U_4 = 0.015$.

From Eq. (14), the overall desirability function for the robust design was then expressed as follows:

$$D_{\mathrm{robust}} = (d_1 \times d_2 \times d_3 \times d_4)^{1/4} \tag{15}$$

where D_{robust} is the overall desirability function for the robust design. The weighing coefficients for all responses were selected as 1.

5. Results and discussions

Fig. 5(a) shows the overall desirability function D_{robust}. It can be seen that there are a lot of zero values for some combines of P and Pos_y. This is because the responses of these combines are out of the "desired" limits of certain single desirability function d_i (i = 1–4) and they are completely unacceptable for the overall desirability function.

From Fig. 5, the overall desirability function is a continuous, nonlinear, piecewise function and therefore a direct search method, downhill simplex search, was used to find the combine

Table 5
The statistic properties of maxσ_z and $\Delta\sigma_z$ of three solutions

	P (MPa)	Pos_y (mm)	maxσ_z (MPa)		$\Delta\sigma_z$ (MPa)	
			Mean	s^a ($\times10^{-2}$)	Mean	s^a ($\times10^{-2}$)
Arbitrary solution	1.2	10	0.4893	1.63	0.2869	1
Optimal solution	1.5	5.7759	0.5677	1.52	0.3104	0.87
Robust solution	1.5	0	0.5098	1.38	0.2517	0.67

[a] S.D.

of the design variables Pos_y and P that maximizes the overall desirability. By maximizing D_{robust}, the robust solution was obtained as -1.4285 for coded value of Pos_y and 1.4285 for coded value of P, that is 0 mm for Pos_y and 1.5 MPa for P with $D_{robust} = 0.5479$ as Fig. 5(a) shows.

To verify the reliability of the robust solution, we found the optimal solution of the assembly parameters, which will not consider the variations in the design variables. From the construction process of D_{robust}, one can see that the desirability function of the optimal design D_{op} for the criteria that maximum maxσ_z and minimum $\Delta\sigma_z$ can be obtained by omitting d_3 and d_4, that is:

$$D_{op} = (d_1 \times d_2)^{1/2} \quad (16)$$

where d_1 and d_2 are the desirability functions of maxσ_z and σ_z.

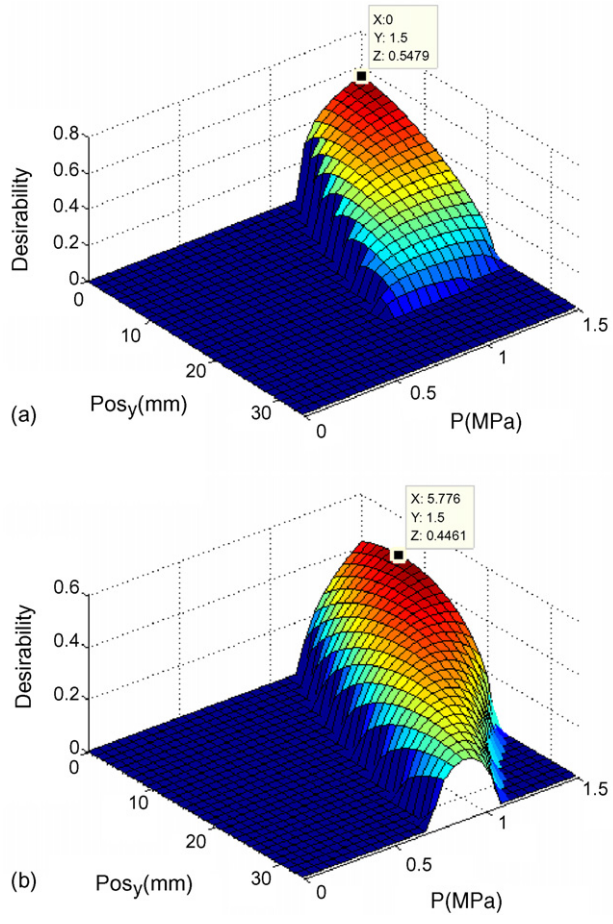

Fig. 5. Contours of the overall desirability functions of (a) robust design and (b) optimal design.

By maximizing D_{op}, the optimum solution was obtained as -0.9359 for coded value of Pos_y and 1.4285 for coded value of P, that is 5.776 mm for Pos_y and 1.5 MPa for P with $D_{op} = 0.4461$. The overall desirability function of optimal solution D_{op} is shown in Fig. 5(b).

An arbitrary combine of the design variables, $Pos_y = 10$ mm and $P = 1.2$ MPa, was also chosen to conduct the validation.

In order to verify the robustness of the robust solution, we compared the performances of the arbitrary solution, optimal solution and robust solution on maxσ_z and $\Delta\sigma_z$. Three sets of normal distributions for P and Pos_y were established with the different mean values but the same variance. The mean values are the arbitrary solution, optimal solution and robust solution, respectively, and the same variances are $\sigma_P = 0.04$ MPa and $\sigma Pos_y = 0.33$ mm. Using PDS again with the three normal distributions of the design variables, three sets of maxσ_z and $\Delta\sigma_z$ can be obtained corresponding to the arbitrary solution, optimal solution and robust solution, respectively.

The statistic properties of maxσ_z and $\Delta\sigma_z$ corresponding to the arbitrary solution, optimal solution and robust solution are listed in Table 5, respectively. As Table 5 shows, the robust solution shows less variability on the maxσ_z and $\Delta\sigma_z$ than both the optimal solution and arbitrary solution. It can be also observed that the robustness has been achieved at the expense of the decrease of mean value of maxσ_z and $\Delta\sigma_z$. In this study, the larger maxσ_z and smaller $\Delta\sigma_z$ the better. In this fashion, the robust solution decreases the value of contact pressure but makes the uniformity better. This can be explained by the competing relationship between the two responses maxσ_z and $\Delta\sigma_z$.

Table 5 also shows the robustness of the robust solution, compared with the optimal solution, for $\Delta\sigma_z$ is better than that for maxσ_z. That is 10.14% standard deviation less on maxσ_z while 29.85% on $\Delta\sigma_z$. This is in accordance with Fig. 4, which also shows the gradient change of maxσ_z is less than that of $\Delta\sigma_z$.

6. Conclusions

A methodology of robust design integrated with FEA, RSM, POE and desirability function has been developed to find the robust solution of the assembly parameters for a PEMFC stack. It has been demonstrated that the proposed robust design scheme is feasible and effective for the assembly parameters considered. For this PEMFC stack, the robust solution shows that the end plate bolts should be at the middle of four margins of the end plate and the assembly pressure should be 1.5 MPa. It also

shows that the assembly pressure plays a more important rule on the MEA pressure distribution than the position of end plate bolts.

The RSM, PDS, POE and desirability function can be useful in the robust design process. Especially, the PDS, which integrated the probability and FEA, can be used to find out the influence of the variations of the design factors. The methodology of the present study can be used to seek robust sets of the assembly parameters for the designers to improve the performance of a PEMFC stack.

In this study, the weighing coefficients for all response variables were selected as the same values 1. However, from the construction process of the overall desirability function, it can be seen that one can change the weighing coefficients to vary the importance of each response variable individually based on individual engineering needs. The model was simplified by assuming isotropic material behavior, however, to make the results more accurate, the anisotropic material behavior should be researched and considered. The model also needs to be experimentally validated. Our research works in the future will be focused on these areas.

Acknowledgements

The work reported here is sponsored by the National High Technology Research and Development Program of China (20060111A1222). The authors gratefully acknowledge the supports.

References

[1] G. Hoogers, Fuel Cell Technology Handbook, CRC Press, Boca Raton, FL, 2003.
[2] V. Mishra, F. Yang, R. Pitchumani, ASME J. Fuel Cell Sci. Technol. 1 (2004) 2–9.
[3] A. Vlahinos, K. Kelly, J. D'Aleo, J. Stathopoulos, First International Conference on Fuel Cell Science Engineering and Technology, Rochester, NY, USA, April 21–23, 2003.
[4] X. Yan, M. Hou, H. Zhang, F. Jing, P. Ming, B. Yi, J. Power Sources 160 (2006) 252–257.
[5] J.-J. Hwang, H.-S. Hwang, J. Power Sources 104 (2002) 24–32.
[6] S.-J. Lee, C.-D. Hsu, C.-H. Huang, J. Power Sources 145 (2005) 353–361.
[7] W.-K. Lee, C.-H. Ho, J.W. Van Zee, M. Murthy, J. Power Sources 84 (1999) 45–51.
[8] Y.-G. Yoon, W.-Y. Lee, G.-G. Park, T.-H. Yang, C.-S. Kim, Electrochim. Acta 50 (2004) 709–712.
[9] P. Zhou, C.W. Wu, G.J. Ma, J. Power Sources 163 (2007) 874–881.
[10] S. Koch, P. Hendriksen, Solid State Ionics 168 (2004) 1–11.
[11] R.H. Myers, D.C. Montgomery, Response Surface Methodology: Process and Product Optimization Using Designed Experiments, 2nd ed., John Wiley and Sons, New York, 1995.
[12] X.K. Gao, T.S. Low, Z.J. Liu, S.X. Chen, IEEE Trans. Magn. 38 (2002) 1141–1144.
[13] S. Reh, J.-D. Beley, S. Mukherjee, E.H. Khor, Struct. Saf. 28 (2006) 17–43.
[14] ANSYS Inc., Probabilistic Design Techniques, Advanced Analysis Techniques Guide, August, 2002.
[15] Y. Chao Liu, Lawrence Yao, J. Manuf. Proc. 4 (1) (2002).
[16] G. Taguchi, Y. Wu, Introduction to Off-Line Quality Control, Central Japan Quality Control Association, 1979.
[17] P.J. Whitcomb, M.J. Anderson, Annu. Qual. Congr. Trans. (1996) 642–651.
[18] G. Derringer, R. Suich, J. Qual. Technol. 12 (4) (1980) 214–219.
[19] I. Eren, F. Kaymak-Ertekin, J. Food Eng. 79 (2007) 344–352.